


## Terahertz Pulse Generation in Underdense Relativistic Plasmas: From Photoionization-Induced Radiation to Coherent Transition Radiation

J. Déchard,<sup>\*</sup> A. Debayle, X. Davoine, L. Gremillet, and L. Bergé  
CEA, DAM, DIF, F-91297 Arpaçon, France

 (Received 13 September 2017; revised manuscript received 25 January 2018; published 4 April 2018)

Terahertz to far-infrared emission by two-color, ultrashort optical pulses interacting with underdense helium gases at ultrahigh intensities ( $>10^{19}$  W/cm<sup>2</sup>) is investigated by means of 3D particle-in-cell simulations. The terahertz field is shown to be produced by two mechanisms occurring sequentially, namely, photoionization-induced radiation (PIR) by the two-color pulse, and coherent transition radiation (CTR) by the wakefield-accelerated electrons escaping the plasma. We exhibit laser-plasma parameters for which CTR proves to be the dominant process, providing terahertz bursts with field strength as high as 100 GV/m and energy in excess of 10 mJ. Analytical models are developed for both the PIR and CTR processes, which correctly reproduce the simulation data.

DOI: [10.1103/PhysRevLett.120.144801](https://doi.org/10.1103/PhysRevLett.120.144801)

In recent years, the generation of terahertz radiation by ultrashort laser pulses has stirred much interest due to many applications in medicine and security [1]. Among other techniques [2–4], frequency conversion through a plasma spot seems particularly promising given the absence of emitter damage and the production of intense broadband fields [5,6]. In laser-gas interactions at moderate pump intensities ( $\sim 10^{14-15}$  W/cm<sup>2</sup>), various mechanisms come into play, depending on the intensity level and the temporal laser profile. While terahertz radiation by single-color laser pulses appears to be mainly mediated by the longitudinal ponderomotive force through transition-Cherenkov emission [7], transverse photocurrents prevail when using temporally asymmetric two-color pulses [6,8,9]. This trend has been verified up to subrelativistic intensities  $\lesssim 10^{18}$  W/cm<sup>2</sup> [10,11].

Moderate pump intensities routinely supply less than 10  $\mu$ J terahertz yields [12], so progress remains to be made toward producing millijoule-level pulses with field strength in the range of gigavolts per meter, which could be helpful for remote sensing applications. Ultrahigh-intensity (UHI) lasers appear well suited in this regard because of their ability to generate strong charged-particle currents. In thin solid foils irradiated at intensities  $>10^{19}$  W/cm<sup>2</sup>, high-energy ( $\sim 500$   $\mu$ J) terahertz pulses associated with conversion efficiencies  $\eta \sim 5 \times 10^{-4}$  have been reported and ascribed either to transient electron or ion currents at the target rear surface [13], or to coherent transition radiation (CTR) by energized electrons escaping the target [14–16]. In under- or near-critical plasmas, it has been found experimentally that terahertz radiation can originate from CTR [17] or linear mode conversion of Langmuir waves excited in nonuniform density profiles [18], both mechanisms leading to relatively low conversion efficiencies ( $\eta \sim 10^{-6}$ ).

In this Letter, we show by means of 3D particle-in-cell (PIC) simulations that gaseous targets driven at intensities  $>10^{19}$  W/cm<sup>2</sup> by two-color pulses in the blowout wakefield regime can also provide efficient ( $\eta > 5 \times 10^{-3}$ ) terahertz to far-infrared sources. Our study reveals that CTR can largely prevail over photoionization-induced radiation (PIR), yielding unprecedented 100 GV/m terahertz field strengths in gases. The simulation results are analyzed in light of the CTR theory and a simplified model of a radiating electron bunch exiting into vacuum. Moreover, we derive an analytical formula for PIR that takes into account the nonlinear density modulations associated with the wakefield. Finally, we assess the dependence of the terahertz emission on the laser and gas parameters.

Our 3D PIC simulations are performed using the CALDER-CIRC code [19], which solves the coupled Vlasov-Maxwell equations including strong-field ionization [20]. In the baseline simulation, a 3.7 J laser pulse, linearly polarized along  $x$  and propagating along the  $z$  axis, is focused into a gas target of helium (He) with initial atomic density  $n_a = 2.4 \times 10^{17}$  cm<sup>-3</sup>, 400  $\mu$ m length ( $L_p$ ), and shaped with 100- $\mu$ m-long density ramps on both sides to mimic the conditions met in gas-jet experiments. In CALDER-CIRC, the electromagnetic fields are discretized on a  $(r, z)$  grid and decomposed over a reduced set of Fourier angular modes ( $\propto e^{im\theta}$ ) around the  $z$  axis. Only the first two modes are retained here. The fundamental  $m = 0$  mode corresponds to axisymmetric fields such as the radially polarized ones. The  $m = 1$  mode contains nonaxisymmetric fields, including the  $x$ -polarized laser field. In order to optimize terahertz emissions [6,8], we consider a two-color laser field composed of a fundamental pulse with carrier wavelength  $\lambda_0 \equiv 2\pi c/\omega_0 = 1$   $\mu$ m (where  $\omega_0$  is the laser angular frequency and  $c$  is the velocity of light) and its second harmonic, shifted

by a relative phase of  $\pi/2$ . The  $2\omega_0/\omega_0$  intensity ratio is 10% for a total laser intensity  $I_0 = 2.2 \times 10^{19}$  W/cm<sup>2</sup>, corresponding to a normalized field strength  $a_0 \equiv eE_0/m_e\omega_0c = 4$  (where  $E_0$  is the electric field strength,  $e$  is the electron charge, and  $m_e$  is the electron mass). The laser harmonics have Gaussian profiles in both space and time with equal initial widths  $w_0 = 20$   $\mu$ m and durations  $\tau_0 = 35$  fs (FWHM). This setup fulfills the conditions for efficient electron blowout ( $w_0\omega_{pe}/c \approx 2\sqrt{2a_0\ln 2}$ ,  $\tau_0 \approx 2w_0/3c$  with  $a_0 \gtrsim 4$ , where  $\omega_{pe}$  is the electron plasma frequency; see Ref. [21]).

The terahertz fields are extracted by filtering the total field spectrum below a cutoff frequency  $\omega_{co} = 0.3\omega_0$  ( $\nu_{co} \equiv \omega_{co}/2\pi = 90$  THz). Attention is paid to the transmitted terahertz fields only, as they usually prevail over the backscattered components in gases [10]. We checked that backward terahertz emissions by resonant transition radiation [22] in the front density ramp remain weak. Inspection of the terahertz field in vacuum shows that the transverse field strength ( $E_\perp$ ) exceeds the longitudinal one ( $E_z$ ) by one order of magnitude. This invites us to restrict our analysis to  $E_\perp$ , whose PIR and CTR components can be discriminated through direct angular expansion: the PIR field is polarized along the laser field [11], and so it is described by the  $m = 1$  mode. By contrast, the wakefield-driven electron bunch is essentially axisymmetric; hence, the resulting CTR (radially polarized) is mainly contained in the  $m = 0$  mode.

Figure 1(a) displays a set of isosurfaces of the PIR (blue color map) and CTR (red color map) electric fields at a distance of 500  $\mu$ m from the rear side of the plasma. The rightward-propagating laser pulse is visualized by the yellow isosurface. A primary PIR burst occurs at a distance of  $\sim 20$   $\mu$ m in front of the laser peak, reaching a maximum amplitude of  $\sim 1$  GV/m on axis and carrying a total energy of 1.3  $\mu$ J. About one plasma wavelength behind the laser pulse, a radially polarized burst produces the maximum terahertz field  $\sim 15$  GV/m, corresponding to a  $\sim 160$   $\mu$ J energy. The location and the hollow conical shape of this emission are consistent with CTR by electrons accelerated in the laser wakefield, as justified below. In the present UHI conditions, this strongly nonlinear plasma wave takes the form of a succession of ion cavities due to radial expulsion of the plasma electrons [21]. The intense burst evidenced in Fig. 1(a) is emitted when the electron bunch that has been trapped in the first cavity exits into vacuum. This scenario is supported by Figs. 1(b) and 1(c), which show the  $m = 0$  component of the longitudinal electron current density ( $J_z$ ), and the electron ( $z, p_z$ ) phase space at time  $t = 2.55$  ps, respectively. The strong peak in  $J_z$  seen at the foot of the density downramp ( $z \simeq 690$   $\mu$ m) corresponds to a high-energy ( $p_z \gtrsim 25m_e c$ ) electron bunch about to exit the plasma. Subsequent cavities also accelerate a few electron packets, yet at lower energies and densities. Finally, Fig. 1(a) reveals a secondary nonaxisymmetric signal on top of the CTR. This emission, less collimated but more

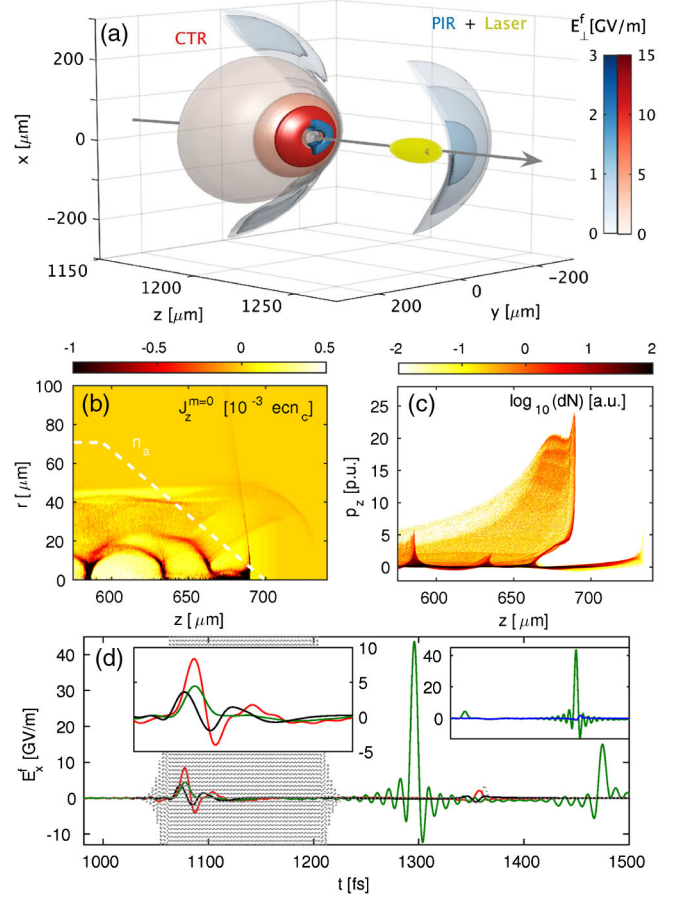


FIG. 1. Terahertz field emission from a He gas target of  $2.4 \times 10^{17}$  cm<sup>-3</sup> atomic density driven by a  $2.2 \times 10^{19}$  W/cm<sup>2</sup>, 35 fs two-color laser pulse. (a) 3D isosurfaces of the filtered ( $\nu < 90$  THz) transverse field ( $E_\perp^f$ ) in vacuum at 500  $\mu$ m from the plasma boundary ( $t = 4.17$  ps). Terahertz radially polarized ( $m = 0$ ) modes are fully displayed (red color map), while terahertz laser-polarized ( $m = 1$ ) modes are shown as half-caps for better readability (blue color map). The yellow isosurface delineates the laser pulse envelope (propagating along the grey arrow) for a normalized field strength  $a = 2/3$  ( $E_\perp = 2140$  GV/m). (b) Snapshot of the  $m = 0$  component of the longitudinal current ( $J_z$ ) at time  $t = 2.55$  ps when the laser pulse exits the plasma (atomic density is visualized by a white dashed line). (c) Electron number ( $dN$  in  $\log_{10}$  scale) in the ( $z, p_z$ ) phase space at the same instant. (d) Time history of the on-axis  $E_x^f$  field at 300  $\mu$ m inside the plasma, as given by the 3D (green curve) and the 1D (red curve) PIC simulations, and the solution of Eq. (1) (black curve). The grey dashed curve corresponds to the laser pulse. The left inset zooms in on the front pulse; the right inset includes the on-axis field from a preionized plasma (blue curve).

intense ( $\sim 3$  GV/m, corresponding to an energy of  $\sim 2.6$   $\mu$ J) than that occurring in the laser front pulse, stems from the coupling of the transverse photocurrents and the strong density oscillations accompanying the wakefield.

To gain insight into the PIR, we plot in Fig. 1(d) the time history of the on-axis filtered  $E_x^f$  field at a depth of 300  $\mu$ m inside the plasma (green curve), and we compare it with the

result of a 1D PIC simulation using the same parameters (red curve). Relatively good agreement (within a factor  $\sim 2$ ) is found between the 1D and 3D curves during the laser pulse [see also left inset of Fig. 1(d)], both showing peak fields of  $\sim 4\text{--}8$  GV/m. Outside the plasma, diffraction causes this primary terahertz emission to weaken as it propagates in vacuum [Fig. 1(a)]. As detailed in the Supplemental Material [23] (using Refs. [24,25]), an expression for the PIR field can be derived in a 1D geometry by assuming an unperturbed laser pulse (indexed by  $L$ ) moving at  $c$  and a stationary plasma wave in the comoving coordinate system ( $\xi = z - ct$  and  $s = t$ ). By introducing the vector potential  $A_x = A_L(\xi) + \delta A_x(\xi, s)$  and transverse momentum  $p_x = p_L(\xi) + e\delta A_x(\xi, s)$  ( $|\delta A_x| \ll |A_L|$ ), the 1D wave equation of the radiated vector potential has the following solution:

$$\delta A_x = \frac{1}{2} \sqrt{\frac{1}{m_e \epsilon_0 c^2}} \int_0^\xi d\xi' \frac{n_e p_L}{\gamma_e}(\xi') \sqrt{\frac{2cs + \xi - \xi'}{\int_{\xi'}^{\xi} \frac{n_e}{\gamma_e} d\xi''}} \times J_1 \left( \sqrt{\int_{\xi'}^{\xi} \frac{e^2 n_e}{m_e c^2 \gamma_e} d\xi'' (2cs + \xi - \xi')} \right), \quad (1)$$

where  $J_1(x)$  is the Bessel function of the first kind,  $\epsilon_0$  is the permittivity of vacuum,  $n_e$  is the electron density, and  $\gamma_e$  is the Lorentz factor associated with the electron velocity  $v_e$ . The electron density is computed numerically from the standard wakefield equation, supplemented with a photoionization source [23]. Equation (1) describes the coupling between the transverse photocurrents, which mediate the usual PIR during the laser pulse [26], and the density modulations associated with both photoionization and the nonlinear laser wakefield. This formula correctly reproduces the 1D PIC result during the laser pulse [see left inset of Fig. 1(d)]. Also, due to the interplay of PIR and wakefield, terahertz bursts occur at each density peak with a  $\sim 250$  fs period, as seen at time  $t \simeq 1360$  fs in both the 1D PIC and theoretical curves. In the 3D simulation, the corresponding emission occurs a bit earlier ( $t \simeq 1300$  fs) and at a much higher amplitude ( $\sim 40$  GV/m vs  $\sim 2$  GV/m in 1D); this is explained by differences in the dynamics and shape of the 1D and 3D plasma waves, the latter being subject to complete electron blowout and 10 times higher peak densities. This signal vanishes in a 3D preionized plasma [see right inset of Fig. 1(d)], hence demonstrating the role of the transverse electron fluid velocity initiated by photoionization. It still prevails over the primary PIR burst in vacuum at  $500 \mu\text{m}$  from the plasma, although it is more strongly reduced by diffraction down to 3 GV/m [Fig. 1(a)]. The PIR process is expected to saturate, since helium atoms are fully ionized early in the pulse front. It could be further boosted by using higher-Z gases, e.g., argon, to promote ionization events throughout the laser pulse [10,11].

We now turn to the analysis of the brightest radially polarized signal measured in vacuum [Fig. 1(a)]. To prove

that it mainly arises from CTR by wakefield-driven electrons, we compare its 2D energy spectrum with that predicted from a pointlike monoenergetic electron bunch exiting perpendicularly to the plasma surface [27–30]:

$$\frac{d^2 W_e}{d\omega d\Omega} = \frac{c N_e^2 e^2 \sin^2 \theta \cos^2 \theta}{\pi^2 v_e^2} \frac{\beta_e^4}{(1 - \beta_e^2 \cos^2 \theta)^2} \times \left| \frac{(\epsilon - 1)(1 - \beta_e^2 - \beta_e \sqrt{\epsilon - \sin^2 \theta})}{(\epsilon \cos \theta + \sqrt{\epsilon - \sin^2 \theta})(1 - \beta_e \sqrt{\epsilon - \sin^2 \theta})} \right|^2. \quad (2)$$

Here,  $d^2 W_e / d\omega d\Omega$  is the radiated energy density per units of angular frequency ( $\omega$ ) and solid angle ( $\Omega$ ),  $\theta$  is the angle between the propagation axis and the observer,  $N_e$  is the number of electrons inside the bunch,  $v_e = \beta_e c$  is their velocity, and  $\epsilon = 1 - \omega_{pe}^2 / \omega^2$  is the plasma dielectric function. The assumption of a pointlike electron bunch holds provided that the bunch size is much smaller than the radiation wavelength, in which case the emission is coherent [30]. Equation (2) can be recast in terms of the longitudinal ( $k_z$ ) and transverse ( $k_r$ ) wave numbers using  $\theta = \arctan(k_r / k_z)$  and  $\omega = c \sqrt{k_z^2 + k_r^2}$ . Figures 2(a) and 2(b) show the terahertz spectra computed from the 3D PIC simulation and from Eq. (2), respectively, using the mean values  $\gamma_e = 1 / \sqrt{1 - \beta_e^2} = 15$  and  $N_e = 8.9 \times 10^8$  that best fit the electron bunch issued from the first wakefield bucket [with  $p_z \geq m_e c$  in Fig. 1(c)]. Despite the crude simplifications of Eq. (2) (e.g., neglecting the electron beam's energy and angle spread), the two spectra fairly agree in intensity and shape: both present a maximum emission along  $\theta_{\max} \simeq \gamma_e^{-1}$  (white dashed line) with a cutoff frequency  $\omega_{\max} \simeq \gamma_e \omega_{pe} \approx 0.3 \omega_0$ , as expected from CTR by relativistic electrons [28]. About 75% of the radiated

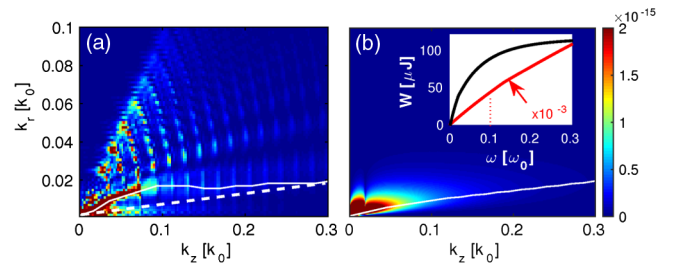


FIG. 2. 2D ( $k_z, k_r$ ) spectrum of the axisymmetric field  $E_{\perp}^f$  in vacuum at  $500 \mu\text{m}$  from the plasma: (a) 3D PIC simulation results. The white solid line plots the angle of maximum emission for each  $k_z$ . The white dashed line shows the asymptotic emission angle  $\theta_{\max} = \gamma_e^{-1}$ . (b) CTR theory [Eq. (2)] for  $\gamma_e = 15$  and  $N_e = 8.9 \times 10^8$ . The inset shows the energy spectrum (in microjoules) integrated from Eq. (2) over the entire solid angle and up to the frequency  $\omega[\omega_0]$  for  $n_a = 2.4 \times 10^{17} \text{ cm}^{-3}$  (black curve) and  $n_a = 97 \times 10^{17} \text{ cm}^{-3}$  (red curve). In the latter case, discussed in Fig. 4(b), the electron bunch parameters are  $\gamma_e = 150$  and  $N_e = 1.06 \times 10^{10}$ .



energy ( $\sim 120 \mu\text{J}$ ) is emitted below 30 THz ( $0.1\omega_0$ ). The PIC spectrum, however, differs from the theoretical one by additional weaker emissions at larger angles and spectral modulations separated by  $\Delta k_r \simeq \omega_{pe}/c$ , which are ascribed to radiation by lower-energy electron bunches produced in the second and third wakefield buckets. The inset of Fig. 2(b) plots the theoretical radiated energy (in microjoules) given by the cumulative  $\omega$  integral of Eq. (2) (black curve). In the terahertz frequency range  $\omega < 0.3\omega_0$ , we obtain a total energy of  $\sim 110 \mu\text{J}$ , comparable with the  $\sim 160 \mu\text{J}$  yield measured in the simulation.

In addition to CTR, the radially polarized terahertz spectrum measured outside the plasma in the PIC simulation also includes the proper field of the electron bunch, which is not described by Eq. (2). This field is of electrostatic character in the bunch rest frame, and should thus be discarded when evaluating the source efficiency in emitting purely electromagnetic terahertz radiations. To model the space-time field distribution resulting from both the plasma-boundary crossing and subsequent propagation of the electron bunch, we make use of the generalized Biot-Savart law [31]:

$$\mathbf{B}(\mathbf{r}, t) = \int d\mathbf{r}' \left\{ \frac{\mathbf{J}(\mathbf{r}', t')}{cR^2} + \frac{1}{c^2 R} \left[ \frac{\partial \mathbf{J}(\mathbf{r}', t')}{\partial t'} \right] \right\} \frac{\mathbf{R}}{R}, \quad (3)$$

where  $\mathbf{B}$  is the magnetic field,  $\mathbf{J}$  is the current density,  $\mathbf{r}$  is the observer's position,  $\mathbf{R} \equiv \mathbf{r} - \mathbf{r}'$ , and the square brackets denote an evaluation at the retarded time  $t' \equiv t - R/c$ . Equation (3) is computed for a monoenergetic electron bunch of zero radius and finite length  $L_e$ , moving at constant velocity along the  $z$  axis [23]. Transition radiation arises from assuming that the beam emerges into vacuum through the plasma surface, which implies that the plasma behaves as a perfect conductor. The specific features of the CTR-like and proper fields are discussed in Ref. [23]. Figure 3 compares the result of Eq. (3) [Fig. 3(b)] with the axisymmetric  $B_\theta$  field measured in the 3D simulation when the main electron bunch has propagated  $500 \mu\text{m}$  beyond the interface [Fig. 3(a)]. In Fig. 3(b), we use the parameter values  $\gamma_e = 15$ ,  $N_e = 8.9 \times 10^8$ , and  $L_e = 1.5 \mu\text{m}$ . Good agreement is found outside the bunch ( $r \gtrsim 30 \mu\text{m}$ ) between the two maps of  $B_\theta$  filtered in the terahertz band  $\nu < 90$  THz, both in amplitude and spatial shape. The main discrepancy is found inside the bunch, for which Eq. (3) overestimates the simulated field due to the assumed zero radius of the bunch, whereas the latter diverges to some extent in the simulation [inset of Fig. 3(a)]. To isolate the CTR in our calculation, we subtract the asymptotic proper field of the bunch [23] from the total field, and plot the result in the inset of Fig. 3(b). From comparison of this graph with the total field distributions of Figs. 3(a) and 3(b), it appears that most of the off-axis (axisymmetric) terahertz emission ( $r \gtrsim 30 \mu\text{m}$ ) indeed originates from the plasma-vacuum interface.

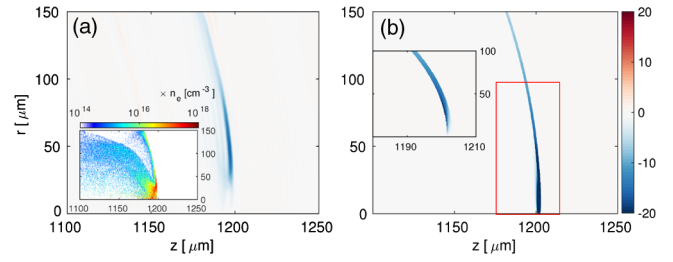


FIG. 3. (a) 2D  $(z, r)$  map of the azimuthal magnetic field,  $cB_\theta$  (in gigavolts per meter), extracted at time  $t = 4.17$  ps from the 3D PIC simulation of Fig. 1. The electron bunch and the plasma-vacuum interface are located at  $z \approx 1200 \mu\text{m}$  and  $z = 700 \mu\text{m}$ , respectively. The inset shows the electron density  $n_e$  (per cubic centimeter). (b) Same quantity as in (a), but given by the Biot-Savart law [Eq. (3)]. The electron bunch parameters are detailed in the text. The inset displays the field emitted from the plasma-vacuum surface, obtained by subtracting the asymptotic proper field of the electron bunch to the total Biot-Savart field. All fields in (a) and (b) are filtered in the frequency range  $\nu < 90$  THz.

The CTR yield evidently depends on the efficiency of the wakefield acceleration, and is therefore sensitive to the laser and gas parameters. Figure 4(a) shows that decreasing the maximum laser field strength to  $a_0 = 1$  leads to a quasilinear plasma wave (with no electron blowout) suppressing particle injection, so that only PIR ( $\sim 1$  GV/m) occurs. Similar field patterns result from a fourfold decrease in the gas density, as displayed in Ref. [23]. At the baseline density, CTR is found to take over PIR from  $a_0 = 2.5$ . Also, the CTR signal can be significantly altered by a change in the density ramp at the rear side of the gas [32]. Finally, Fig. 4(b) illustrates the case of a 40 times denser gas ( $n_a = 97 \times 10^{17} \text{ cm}^{-3}$ ) with a  $100\text{-}\mu\text{m}$ -long ramp. This setup leads to stronger wakefields, still in the blowout regime. As the plasma length remains shorter than the dephasing length ( $L_p = 400 \mu\text{m} < L_d = 2\omega_0^2 w_0 / 3\omega_{pe}^2 \approx 800 \mu\text{m}$ ), there result electron bunches of larger charge and energy ( $N_e \simeq 1.06 \times 10^{10}$  and  $\gamma_e \simeq 150$ ), thus generating via CTR an unprecedented terahertz signal with  $\sim 100$  GV/m field strength and  $\sim 29$  mJ energy yield. These values are consistent with the theoretical CTR spectrum carrying  $\sim 43$  mJ displayed in the inset of Fig. 2(b). In this situation, the emission is coherent mainly

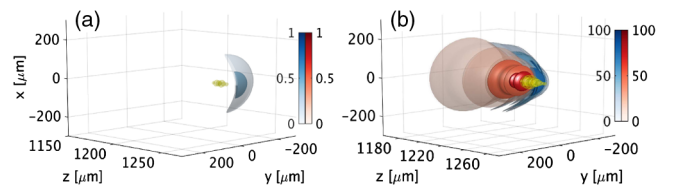


FIG. 4. 3D isosurfaces of the terahertz transverse field ( $E_\perp^f$ ) at  $500 \mu\text{m}$  from the plasma-vacuum interface for different laser-gas parameters: (a)  $a_0 = 1$ ,  $n_a = 2.4 \times 10^{17} \text{ cm}^{-3}$  and (b)  $a_0 = 4$ ,  $n_a = 97 \times 10^{17} \text{ cm}^{-3}$ . Red (blue) color maps correspond to axisymmetric (nonaxisymmetric) fields.

in the frequency range  $\omega < 0.1\omega_0$ , as the longitudinal bunch length is  $\gtrsim 10 \mu\text{m}$  [30]. Most of the terahertz energy (22 mJ) is confined below 10 THz ( $0.033\omega_0$ ). Note that the observed one (two) order(s) of magnitude increase in the field strength (energy) agrees with the linear scaling in  $\gamma_e$  expected from CTR theory [28,33].

In summary, by means of full-scale 3D PIC simulations, we have evidenced the sequential production of intense terahertz bursts using two-color UHI ultrashort laser pulses interacting with He gases of submillimeter lengths and  $>10^{17} \text{cm}^{-3}$  atomic densities. Following a primary terahertz burst induced by photocurrents, CTR at the rear plasma boundary by wakefield-driven relativistic electrons can generate terahertz pulses of  $\sim 100 \text{GV/m}$  field strengths and tens of millijoule energies using relatively modest laser parameters ( $\sim 4 \text{J}$  in energy,  $2.2 \times 10^{19} \text{W/cm}^2$  in intensity), which corresponds to record conversion efficiencies  $\eta > 5 \times 10^{-3}$ . We have obtained an analytical formula that captures the on-axis patterns of the gigavolts-per-meter-level PIR predicted by 1D and 3D simulations. Moreover, analytical CTR models satisfactorily match the simulated radiation in terms of spectral and field distributions. Finally, we have gauged the sensitivity of the CTR and PIR to the interaction setup by varying several laser and gas parameters. Further studies should focus on the electron acceleration stage to provide even more powerful terahertz sources.

The authors acknowledge GENCI, France for awarding us access to the supercomputer CURIE using Grant No. A0010506129.

---

\*jeremy.dechard@cea.fr

- [1] M. Tonouchi, *Nat. Photonics* **1**, 97 (2007).
- [2] W. L. Chan, J. Deibel, and D. M. Mittleman, *Rep. Prog. Phys.* **70**, 1325 (2007).
- [3] C. Vicario, B. Monoszlai, and C. P. Hauri, *Phys. Rev. Lett.* **112**, 213901 (2014).
- [4] A. G. Stepanov, L. Bonacina, S. V. Chekalin, and J.-P. Wolf, *Opt. Lett.* **33**, 2497 (2008).
- [5] D. J. Cook and R. M. Hochstrasser, *Opt. Lett.* **25**, 1210 (2000).
- [6] K. Y. Kim, A. J. Taylor, J. H. Glowia, and G. Rodriguez, *Nat. Photon.* **2**, 605 (2008).
- [7] C. D. Amico, A. Houard, S. Akturk, Y. Liu, J. L. Bloas, M. Franco, B. Prade, A. Couairon, V. Tikhonchuk, and A. Mysyrowicz, *New J. Phys.* **10**, 013015 (2008).
- [8] I. Babushkin, S. Skupin, A. Husakou, C. Köhler, E. Cabrera-Granado, L. Bergé, and J. Herrmann, *New J. Phys.* **13**, 123029 (2011).
- [9] V. A. Andreeva, O. G. Kosareva, N. A. Panov, D. E. Shipilo, P. M. Solyankin, M. N. Esaulkov, P. González de Alaiza Martínez, A. P. Shkurinov, V. A. Makarov, L. Bergé, and S. L. Chin, *Phys. Rev. Lett.* **116**, 063902 (2016).
- [10] A. Debayle, P. González de Alaiza Martínez, L. Gremillet, and L. Bergé, *Phys. Rev. A* **91**, 041801 (2015).
- [11] P. González de Alaiza Martínez, X. Davoine, A. Debayle, L. Gremillet, and L. Bergé, *Sci. Rep.* **6**, 26743 (2016).
- [12] T. I. Oh, Y. S. You, N. Jhajj, E. W. Rosenthal, H. M. Milchberg, and K. Kim, *Appl. Phys. Lett.* **102**, 201113 (2013).
- [13] A. Gopal, S. Herzer, A. Schmidt, P. Singh, A. Reinhard, W. Ziegler, D. Brömmel, A. Karmakar, P. Gibbon, U. Dillner *et al.*, *Phys. Rev. Lett.* **111**, 074802 (2013).
- [14] G. Q. Liao, Y. T. Li, Y. H. Zhang, H. Liu, X. L. Ge, S. Yang, W. Q. Wei, X. H. Yuan, Y. Q. Deng, B. J. Zhu *et al.*, *Phys. Rev. Lett.* **116**, 205003 (2016).
- [15] J. van Tilborg, C. B. Schroeder, C. V. Filip, C. Tóth, C. G. R. Geddes, G. Fubiani, R. Huber, R. Kaindl, E. Esarey, and W. P. Leemans, *Phys. Rev. Lett.* **96**, 014801 (2006).
- [16] A. Pukhov and T. Tüekmantel, *Phys. Rev. ST Accel. Beams* **15**, 111301 (2012).
- [17] W. P. Leemans, C. G. Geddes, J. Faure, C. Tóth, J. van Tilborg, C. B. Schroeder, E. Esarey, G. Fubiani, D. Auerbach, B. Marcellis *et al.*, *Phys. Rev. Lett.* **91**, 074802 (2003).
- [18] G. Q. Liao, Y. T. Li, C. Li, L. N. Su, Y. Zheng, M. Liu, W. M. Wang, Z. D. Hu, W. C. Yan, J. Dunn *et al.*, *Phys. Rev. Lett.* **114**, 255001 (2015).
- [19] A. F. Lifschitz, X. Davoine, E. Lefebvre, J. Faure, C. Rechatin, and V. Malka, *J. Comp. Phys.* **228**, 1803 (2009).
- [20] R. Nuter, L. Gremillet, E. Lefebvre, A. Lévy, T. Ceccotti, and P. Martin, *Phys. Plasmas* **18**, 033107 (2011).
- [21] W. Lu, C. Huang, M. Zhou, M. Tzoufras, F. S. Tsung, W. B. Mori, and T. Katsouleas, *Phys. Plasmas* **13**, 056709 (2006).
- [22] C. Miao, J. P. Palastro, and T. M. Antonsen, *Phys. Plasmas* **23**, 063103 (2016).
- [23] See Supplemental Material at <http://link.aps.org/supplemental/10.1103/PhysRevLett.120.144801> for detailed analytical calculations.
- [24] B. A. Shadwick, C. B. Schroeder, and E. Esarey, *Phys. Plasmas* **16**, 056704 (2009).
- [25] M. V. Ammosov, N. B. Delone, and V. P. Krařnov, *Sov. Phys. JETP* **64**, 1191 (1986).
- [26] A. Debayle, L. Gremillet, L. Bergé, and C. Köhler, *Opt. Express* **22**, 13691 (2014).
- [27] G. M. Garibian, *Sov. Phys. JETP* **6**, 1079 (1958).
- [28] J. D. Jackson, *Classical Electrodynamics* (Wiley, New York, 1975).
- [29] J. Zheng, K. A. Tanaka, T. Miyakoshi, Y. Kitagawa, R. Kodama, T. Kurahashi, and T. Yamanaka, *Phys. Plasmas* **10**, 2994 (2003).
- [30] C. B. Schroeder, E. Esarey, J. van Tilborg, and W. P. Leemans, *Phys. Rev. E* **69**, 016501 (2004).
- [31] U. Bellotti and M. Bornatici, *Am. J. Phys.* **64**, 568 (1996).
- [32] S. Bulanov, N. Naumova, F. Pegoraro, and J. Sakai, *Phys. Rev. E* **58**, R5257 (1998).
- [33] L. Durand, *Phys. Rev. D* **11**, 89 (1975).